A Model of Spike Initiation in Neocortical Pyramidal Neurons

Zachary F. Mainen,*†∥ Jasdan Joerges,*
John R. Huguenard,§ and Terrence J. Sejnowski*‡
*Howard Hughes Medical Institute
Computational Neurobiology Laboratory
Salk Institute for Biological Studies
La Jolla, California 92037
†Neurosciences Graduate Program
‡Department of Biology
University of California, San Diego
La Jolla, California 92093
§Department of Neurology
Stanford University
Stanford, California 94305

Summary

Neocortical pyramidal cells possess voltage-dependent dendritic sodium channels that promote propagation of action potentials into the dendritic tree but paradoxically may fail to originate dendritic spikes. A biophysical model was constructed to reconcile these observations with known anatomical and physiological properties. When dendritic and somatic sodium channel densities compatible with electrophysiological measurements were combined with much higher densities in the axon initial segment then, regardless of the site of stimulation, spikes initiated at the initial segment and subsequently invaded the dendrites. The lower initial segment threshold arose from high current density and electrical isolation from the soma. Failure of dendritic channels to initiate spikes was due to inactivation and source-load considerations, which were more favorable for conduction of back-propagated spikes.

Introduction

The dendrites of central neurons contain a variety of voltage-gated ion channels that may be critical to the processing of electrical signals. In particular, the presence of fast voltage-dependent Na^+ channels in neocortical pyramidal cell dendrites (Huguenard et al., 1989; Stuart and Sakmann, 1994) suggests that these channels may not only underlie long-distance axonal propagation but also shape dendritic function. In the subthreshold regime, dendritic Na^+ channels can be activated by local excitatory synaptic potentials (Magee and Johnston, 1995), indicating that active Na^+ currents may amplify distal synaptic events. In the superthreshold regime, synaptic potentials may not only serve to initiate Na^+ spikes at various loci, but may themselves be affected by action potentials invading the dendrites (Jester et al., 1995). A full grasp of the

interplay between synaptic and voltage-gated currents will clearly require a detailed understanding of the nature of spike initiation and propagation.

Two recent studies of neocortical pyramidal cells have provided conflicting evidence concerning the impact of dendritic Na^+ channels on the initiation of action potentials in neocortical pyramidal neurons. Using voltage-clamp techniques, Regehr et al. (1993) concluded that distal synaptic activation can initiate dendritic spikes far from the soma. By contrast, Stuart and Sakmann (1994), using simultaneous dendritic and somatic recordings, found little evidence for dendritic spike initiation following either electrical or synaptic stimulation of the dendrite. Nevertheless, dendritic Na^+ conductances substantially boosted the invasion of action potentials from the soma back into the dendrites (Stuart and Sakmann, 1994).

To help resolve these issues, we constructed a computer model of action potential generation using independent constraints from anatomical, physiological, and molecular data on neocortical pyramidal cells. Our main goals were to explain the paradoxical ability of dendritic Na^+ channels to support propagation but not initiation of dendritic spikes, to examine the role of the axon initial segment in spike initiation, and to determine the conditions that might lead to ectopic spike initiation.

Results

We examined many different combinations of Na^+ channel kinetics and distributions, in an effort to reproduce the findings of Stuart and Sakmann (1994), and arrived at a model that could account for their main observation, active back-propagation without local initiation of dendritic spikes. The model combined detailed reconstructions of dendritic (Figure 1A) (D. K. Smetters and S. Nelson, unpublished data) and axonal anatomy (Figure 1B) (Fariñas and DeFelipe, 1991) of neocortical pyramidal cells with Na^+ channel kinetics measured in dissociated neocortical neurons (Figure 2) (Huguenard et al., 1988; Hamill et al., 1991). A high density of Na^+ channels in the axon initial segment, compared with the soma and dendrites, was suggested by a variety of data and proved to be critical to the results.

Current injection at either the soma or at points along the apical dendritic shaft evoked action potentials that originated near the soma and then invaded the dendritic site (Figure 3A). The speed of the dendritically propagating spike and the decrement of its amplitude with distance from the soma (Figures 3B and 3C) (compare to figures 1d and 2d in Stuart and Sakmann, 1994) were used to calibrate the somatic/dendritic Na^+ channel density in the model. The value obtained in this manner ($2–3$ μm^{-2}) was comparable to those estimated by outside-out dendritic patch recordings (Stuart and Sakmann, 1994; for a discussion of these density estimates, see Experimental Procedures, this study). That this density of Na^+ channels greatly enhanced the invasion of back-propagating spikes can
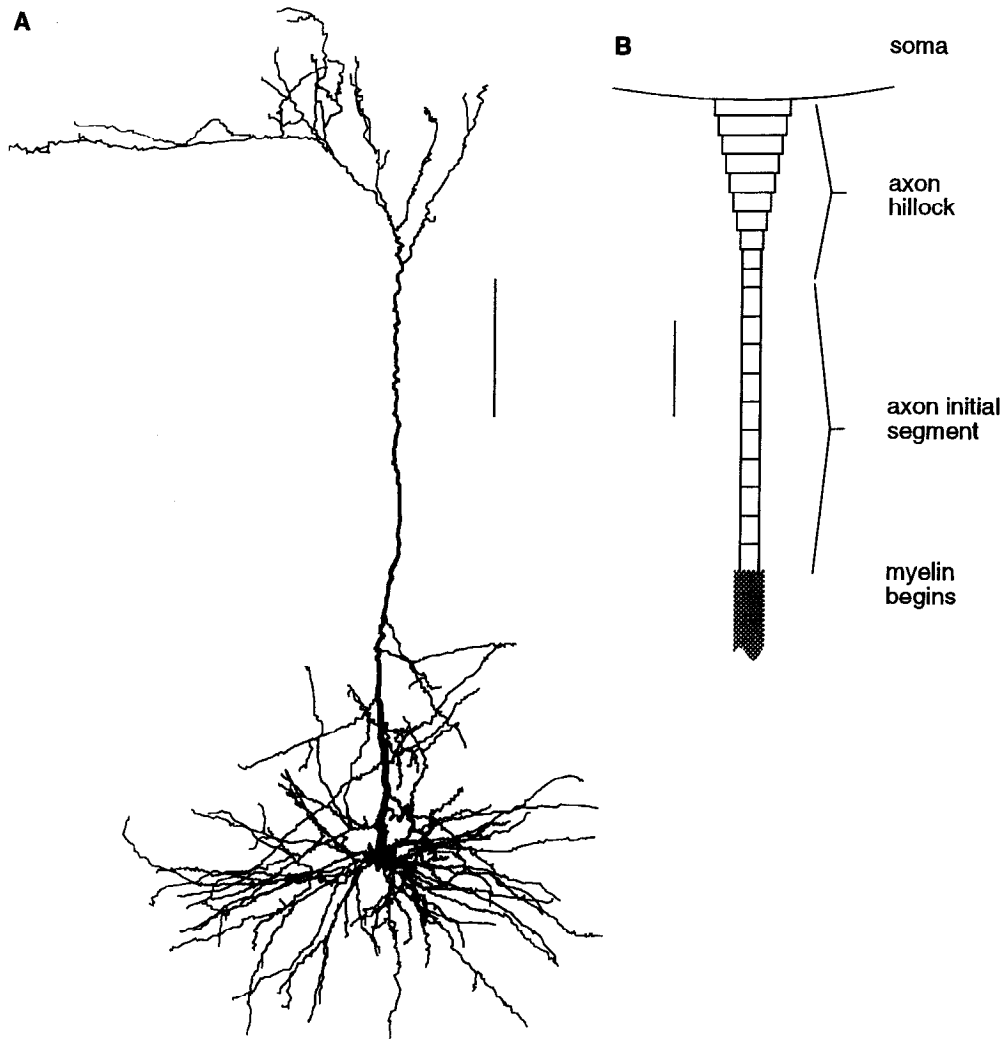
Figure 1. Anatomy of Dendritic Arbor and Axon Hillock and Initial Segment

(A) Dendritic morphology of a rat layer 5 pyramidal cell recorded, filled, and reconstructed by D. K. Smetters and S. Nelson (unpublished).
(B) Geometry of the initial segment used in the model, based on three-dimensional serial electron microscopy reconstructions from cat layer 5 pyramidal cells (Fariñas and DeFelipe, 1991). We refer to the proximal 10 μm of the initial segment, which tapers from 4 μm in diameter to 1 μm, as the "hillock" and the distal 15 μm as the "initial segment." Scale bars are 100 μm (A) and 5 μm (B).

be seen by comparing the peak dendritic depolarization produced by a back-propagating action potential in models with active and passive apical dendrites (Figure 4).

The ability of low densities of Na$^+$ channels to conduct but not to initiate action potentials can be partly explained by considering Na$^+$ channel inactivation (Figure 5). Because the density of Na$^+$ channels in the somatic and dendritic membrane was low relative to the passive electrical load, threshold voltage in these regions was high. Because Na$^+$ channel inactivation began at voltages below this threshold with a speed comparable to the membrane time constant, substantial Na$^+$ inactivation occurred while the dendrite was being charged, greatly reducing the number of available Na$^+$ channels. In contrast, a spike invading the dendrite from the soma depolarized the membrane more rapidly, thus mitigating the effects of inactivation. This behavior is illustrated by plotting the time course of Na$^+$ channel inactivation (the Hodgkin–Huxley "h" parame-

ter) at the dendrite and soma during dendritic versus somatic stimulation (Figure 5).

Inactivation does not completely account for these observations, in that large and brief dendritic current pulses (1–20 nA, 0.5 ms) also failed to initiate dendritic action potentials (data not shown). Although these stimuli can easily produce dendritic voltage transients larger than those produced by a back-propagating action potential, they do not mimic well the electrical effects of the action potential. A spike initiated in the axon charges the soma and proximal dendrites before reaching more distal sites in the apical dendrite, while a dendritic current pulse first charges the local dendritic membrane. When comparable dendritic voltages are reached in the former case, a large portion of the cell's membrane has been depolarized, while in the latter, only the local dendritic region has been. Low densities of dendritic Na$^+$ channels are sufficient to boost a spike traveling from a depolarized region, but not to
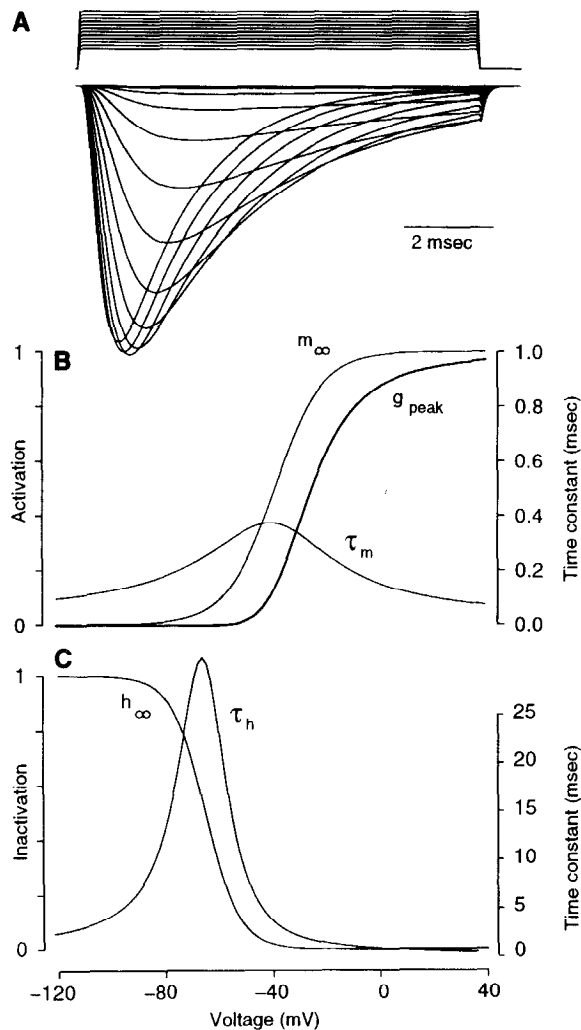
Figure 2. I_{Na} Kinetics

(A) Simulation of Na^+ currents from a series of voltage clamp steps (V_{hold} = 90 mV, V_{clamp} = -60 to 0 mV). The current amplitude scale is arbitrary. For the Na^+ channel density used in the standard model in the dendrites and soma (30 pS/μm^2), the peak current observed was ~1 pA/μm^2.

(B) Steady state (m_∞) and time constant (τ_m) of Na^+ channel activation are plotted as a function of membrane voltage (see equations 2 and 3 in text). The voltage dependence of peak Na^+ conductance (thick line), derived from the simulation above, is also shown

(C) The voltage dependence of steady-state Na^+ inactivation (h_∞) and inactivation time constant (τ_h).

produce equally strong regenerative currents from a resting state.

Contribution of the Axon Initial Segment

The actual site of action potential initiation, as determined by simultaneous somatic and axonal recordings (Stuart and Sakmann, 1994), is in the axon, some distance from the soma. Consistent with this observation, in the model the site of initiation was ~25 μm from the soma, toward the end of the initial segment near the first myelinated internodal segment (Figure 6). Depending on the

electrical space constant of the axon, about which there is some amount of uncertainty, this locus moved further out in the axon or closer to the soma. This is consistent with previous suggestions that the site of initiation in spinal motoneurons may sometimes be at the first node rather than the initial segment (Coombs et al., 1957; Gogan et al., 1983). There was relatively little dependence of the site of initiation on the location of stimulation, consistent with the similarity of behavior with somatic and dendritic current injection.

The axon hillock and initial segment contributed significantly to the size and shape of the action potential seen at the soma. The somatic membrane of the model contained a low density of Na^+ channels, equal to the density in the dendritic membrane (see Huguenard et al., 1988; Stuart and Sakmann, 1994). The current underlying an action potential in the soma was actually supplied largely by Na^+ channels in the initial segment, particularly the proximal portion (the hillock), which was closest electrotonically to the soma. This could be demonstrated by simulations in which the hillock Na^+ channel density was set to 0. In addition, the sharpness of the voltage inflection at the beginning of the action potential was a consequence of initiation in the initial segment. Simulations in which the axon was truncated after the hillock produced slowly rising action potentials that originated in the hillock. Simulations in which Na^+ channels in the basal dendrites were removed showed that these channels also contributed to the somatic action potential amplitude, although their contribution was small compared with that of the initial segment.

Because of the lower threshold for spike initiation, it has been suggested that initial segment Na^+ channel kinetics may have a voltage-dependence that is more negative than those of the soma (Coombs et al., 1957; Dodge and Cooley, 1973). We therefore examined the effect of shifting the voltage dependence of dendritic and somatic Na^+ channel kinetics +5 to +15 mV. We found that such shifts increased the amplitude of dendritic action potentials but were not sufficient in themselves to account for the data in Figure 3 without a large difference between dendritic and axonal channel density.

The low threshold of the initial segment can be understood by comparing the passive (capacitive) load to the magnitude of the source current (Na^+ conductance; Moore et al., 1983). The larger the ratio of source to load, the more quickly the source may charge and thereby depolarize the local membrane. The high density of Na^+ channels in the initial segment provided a very large source current, while its small diameter gave minimal local capacitive load and strong electrical isolation from the load of the soma. By systematically varying the initial segment properties, it was possible to assay which electrical and anatomical features were most important in its contribution to reduced threshold (Figure 6C). Threshold depended mainly on the axial resistivity (R_{ax}), length, diameter, and Na^+ channel density of the initial segment. The relationships between these parameters and threshold level were similar to those expected on the basis of the steady-state electrotonic at-
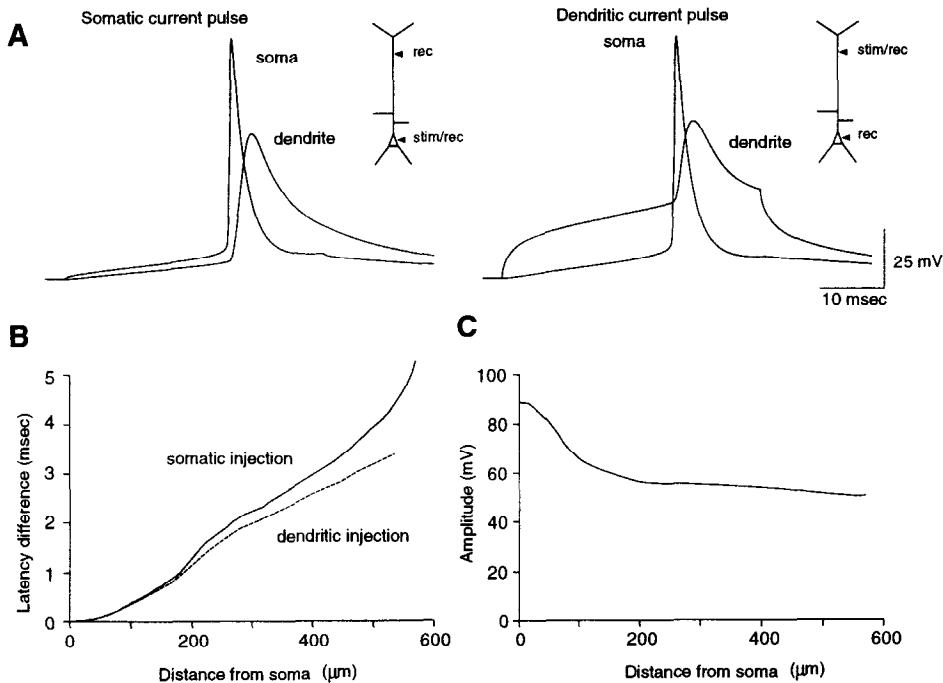
Figure 3. Site of Action Potential Initiation

(A) Voltage traces from the soma and apical dendrite. The dendritic site was on the main apical trunk 416 µm from the soma. The same site was also used in all subsequent figures involving dendritic recording unless otherwise noted. Action potentials were evoked by current steps to either the soma (left, 170 pA) or dendrite (right, 210 pA). The insets in this and following figures show a schematic diagram of the simulated recording and stimulation sites.

(B) Plot of the latency difference between peak somatic and peak dendritic potential at different distances from the soma. Action potentials were elicited by somatic (solid line, 170 pA) or dendritic (dashed line, 100 pA) current injection. Latencies were measured using time to peak amplitude.

(C) Action potential amplitude plotted as function of distance from the soma under the same conditions as (B) following somatic injection. Amplitudes were measured from threshold to peak. Threshold level was determined using the second derivative of membrane potential.

tenuation between the soma and the distal end of the initial segment. In contrast, threshold level was insensitive to the specific membrane capacitance (C_m) and the membrane resistivity (R_m) of the initial segment within an order of magnitude range around the standard parameter values. This observation indicates that the load of the soma and basilar dendritic tree on the initial segment is much larger than the local load of the initial segment itself.

The electrical isolation of the initial segment from the soma may have significant physiological and experimental consequences. Uncontrolled action potentials were initiated readily in the initial segment by simulated somatic voltage clamp steps to superthreshold potentials (Figure 7A). These action potentials always propagated down the axon. Although the amount of voltage escape of the somatic membrane potential from the command potential
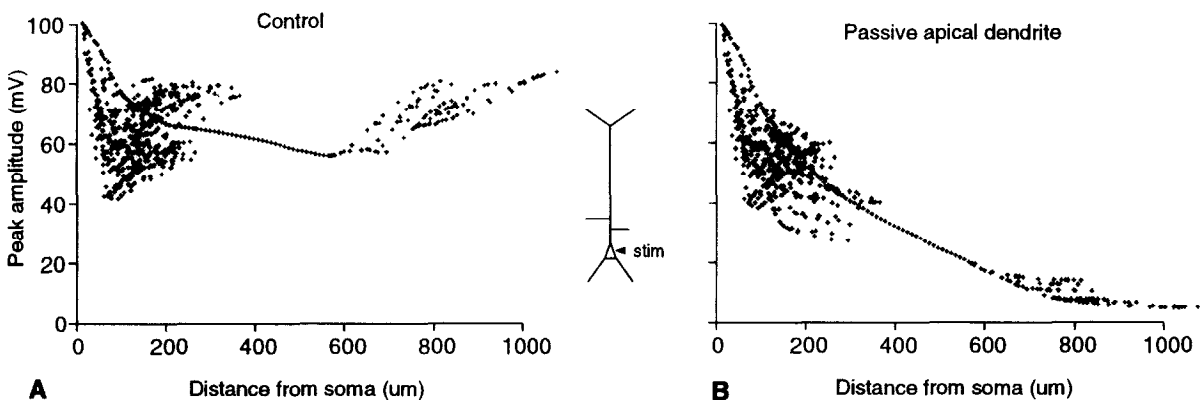

Figure 4. Dendritic Back-Propagation

(A) A current step (170 pA) was injected into the soma of the standard model. For each dendritic segment of the model, the peak voltage is plotted. The scatter of points reflects the different amounts of attenuation at locations in different dendritic branches.

(B) The same protocol is applied when Na^+ channels are removed from the apical dendrite (but not the basal dendrites or soma).
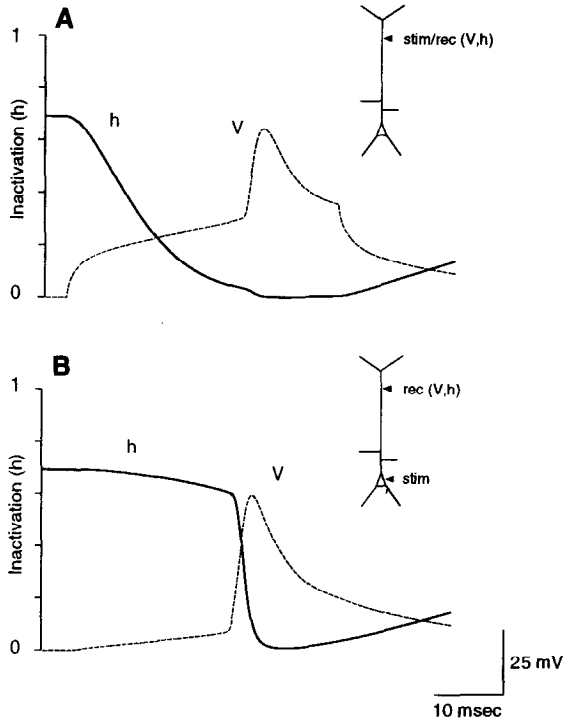
Figure 5. Effect of Na⁺ Channel Inactivation on Action Potential Initiation

A current step was applied to either the soma ([B], 170 pA) or dendrite ([A], 210 pA). Membrane potential and Na⁺ inactivation at the same dendritic site are shown for these two stimulus locations. The inactivation trace corresponds to the Hodgkin–Huxley "h" parameter, which has a range from 0 to 1 (0 indicates all channels are inactivated). The fraction of available Na⁺ channels at the time the spike is triggered is much greater when the action potential is evoked by somatic compared with dendritic current injection.

depended on the series resistance of the clamp, initiation in the initial segment occurred even during "ideal" somatic clamp (series resistance approaching 0). Uncontrolled action potential initiation in the initial segment could also be seen when the soma was clamped during dendritic current injection (see below).

Dendritic Back-Propagation

For an action potential initiated in the axon, the junction between axon and soma in the pyramidal neuron presents an enormous increase in electrical load and drop in Na⁺ current source. The ratio of soma area to initial segment area ($\sim 1500{:}125$ μm^2) and the ratio of soma diameter to initial segment diameter ($\sim 15{:}1$ μm) exceed an order or magnitude. When the basal dendrites are taken into account, the load increase is even larger. Nevertheless, action potentials have been reported to invade readily the somata of pyramidal neurons from the axon even when the soma is not otherwise depolarized (e.g., Cowan and Wilson, 1994).

In the model, action potentials initiated at a distant axonal location successfully invaded the soma when the cell was at rest (Figure 8A). The localization of Na⁺ channels in the initial segment was crucial to this behavior. When the same total channel count (product of channel density

and membrane area) was redistributed uniformly through the soma, hillock, and initial segment, antidromic invasion of the soma did not occur (Figure 8B). The geometry of the initial segment was also important to antidromic invasion. When the normal taper of the axon hillock was replaced by a uniform cylinder abutting the soma, the action potential amplitude in the soma decreased substantially (Figure 8C). This manipulation caused a similar reduction in action potential amplitude when spikes were evoked by dendritic or somatic current injection. Thus, "orthodromic" action potentials were really "antidromic" in some sense, being triggered in the initial segment and subsequently invading the soma and then dendrites. The amplitude of the action potential a few hundred micrometers from the soma into the apical dendrite was not significantly reduced even when the somatic spike amplitude was greatly attenuated, indicating an "all-or-none" aspect to the dendritic invasion of the action potential.

Scenarios for Dendritic Spike Initiation

In contrast to Stuart and Sakmann (1994), Regehr et al. (1993) described synaptically triggered action potentials in the dendrites of cortical pyramidal neurons. Their experiments were performed by voltage clamping the soma; the presence of dendritically initiated action potentials was inferred by the ability of synaptic stimulation to elicit unclamped active currents, presumably occurring in distal, unclamped dendritic regions. We approximated these experimental conditions by injecting current into the apical dendrite while simulating a somatic voltage clamp. In this situation, an action potential could indeed be initiated in the very distal part of the apical dendrite. However, the action potential failed to propagate down the apical dendrite, and the corresponding voltage clamp current recorded at the soma was minimal, indicating a mismatch between model and experiment.

The study of Regehr et al., 1993, was performed using older animals than that of Stuart and Sakmann, 1994 (14–27 days compared with 14 days), and during the second and third weeks of maturation, significant increases in Na⁺ channel density are known to occur (Huguenard et al., 1988; Hamill et al., 1991; Cummins et al., 1994). We reasoned that increased dendritic Na⁺ channel density could be partly responsible for the discrepancy between the two studies; we therefore examined the impact of such an increase by performing simulations with increased somatic and dendritic Na⁺ channel density. With a 3-fold increase in somatic and dendritic channel density (to 90 pS/μm^2), the results of simulations were in much closer accord with the data of Regehr et al., 1993 (Figure 9A, this study). Dendritic current steps evoked either small or large regenerative currents. The small currents corresponded to dendritically initiated action potentials, while the large currents corresponded to axonally initiated action potentials. As reported by Regehr et al. (1993), the series resistance of the clamp was critical to whether or not an axonally initiated spike occurred. With better voltage control, the somatic clamp prevented the initial segment from depolarizing sufficiently to reach threshold. Developmental increases in other channels may be expected to accompany
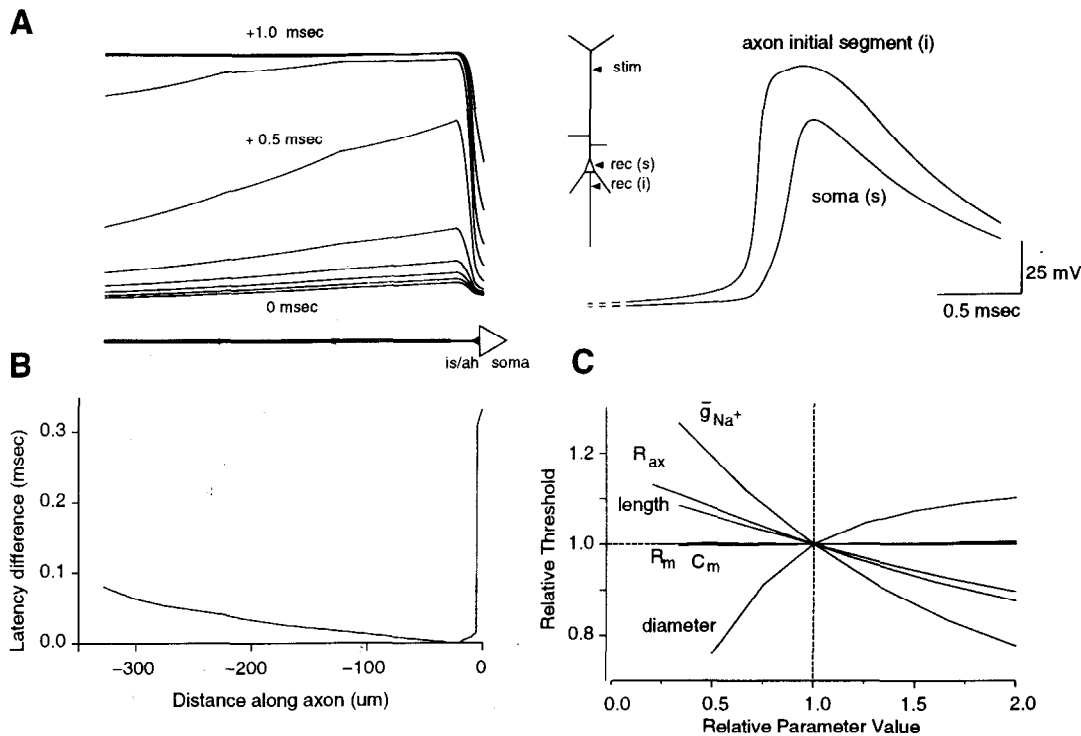
A

B

C

Figure 6. Role of Initial Segment in Action Potential Initiation

(A) Plot of membrane potential as a function of time (right) and space (left). Action potentials were initiated by current injection into the dendrite. The traces on the left plot membrane potential across the axon at a series of time points to show the site of initiation. The traces on the right show the membrane voltage time course at the soma and the distal end of the initial segment. The label "is/ah" indicates the initial segment and axon hillock.

(B) Plot of the difference in action potential latency as a function of distance from the soma along the axon. Latency was determined using the peak curvature of the voltage on the rising phase of the action potential. Simulations were run with a time step of 1 μs.

(C) Effects of initial segment properties on action potential threshold. Current steps were injected into the soma, and the model parameters (length, diameter, axial resistivity R_{ax}, membrane resistivity R_m, and membrane capacitance C_m, as indicated) of the initial segment were varied to produce the curves shown. The threshold level and the parameter values are shown normalized to the standard model (see Table 2). Similar results were obtained using dendritic rather than somatic current injection. Threshold was measured as the somatic voltage at maximum somatic voltage curvature and had a value of 11.6 mV in the standard model. The total number of Na^+ channels (the product of membrane area and channel density) was conserved when length and diameter were varied.

increases in Na^+ channel density (Hamill et al., 1991). Therefore, we performed the same voltage-clamp simulations with a complementary 3-fold increase in somatic and dendritic K^+ channel density. Similar results to those in Figure 9 were found.

With the increased dendritic Na^+ channel density, dendritic current steps in the absence of voltage clamp readily evoked action potentials of dendritic origin (Figure 9B; compare to Figure 3A). Following dendritically originated spikes, the initial segment eventually reached threshold to produce a secondary spike that subsequently propagated back into the dendrites. Thus, the dendritic recording showed a characteristic biphasic waveform, with the first component corresponding to the direct dendritically initiated action potential and the second component corresponding to the back-propagated axonal action potential. Interestingly, the back-propagated action potential produced a greater peak depolarization in the dendrite than the original dendritically initiated action potential. In general, with the higher density of dendritic channels, action potential amplitude did not attenuate with distance from the soma and was actually larger in dendritic than in somatic regions.

Because the density of Na^+ channels in fine caliber dendrites has not been measured directly, localized "hot spots" of Na^+ channels in these dendritic branches are an alternative mechanism for dendritic spike initiation (Softky, 1995). Such hot spots would be likely sites for initiation due to considerations of current source to electrical load similar to those that make the initial segment a likely initiation site. To explore the behavior of the model in such conditions, we simulated loci of high channel density (ten times the normal dendritic density) in small diameter dendritic branches and applied current steps to the apical dendrite (Figure 10). Action potentials could be easily initiated at hot spots located in distal apical dendrites but not readily at hot spots in more proximal oblique apical or basal branches. Spikes initiated at distal hot spots were small but visible in the apical dendrite but barely visible at the soma.

A

clamp command

clamp current

clamp/rec
rec

25 mV
10 nA

3 msec

B

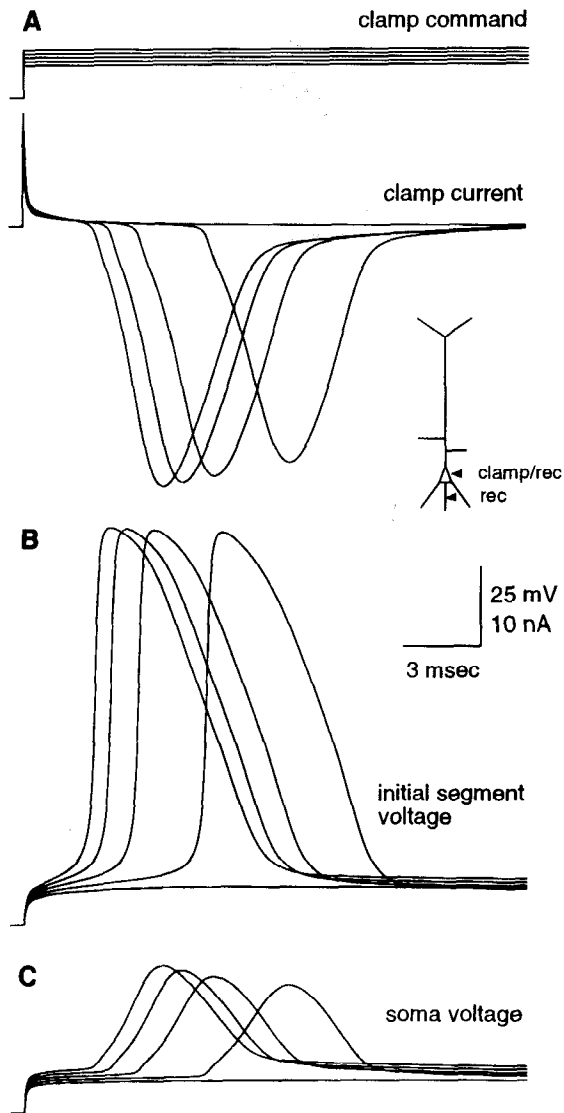initial segment
voltage

C

soma voltage

Figure 7. Voltage Clamp Fails to Prevent Action Potential Initiation in Initial Segment

(A) Somatic voltage clamp steps of +10 to +15 mV from resting potential (from −70 mV) were simulated (upper). Despite low simulated series resistance (1 MΩ), the clamp showed large inward current responses (lower) due to triggering of action potentials in the initial segment.

(B) The initial segment was not well space-clamped due to its electrical isolation from the soma.

(C) The somatic membrane potential also showed voltage escape due to the finite series resistance of the clamp.

Discussion

We have presented a model of action potential initiation in neocortical pyramidal cells that is consistent with the known physiological and anatomical properties of these cells. In this model, the axon initial segment is the usual trigger zone for spikes by virtue of its geometry and high Na^+ channel density. The surprising ability of dendritic Na^+ channels to substantially boost back-propagation of action potentials while failing to support dendritic initiation (Stuart and Sakmann, 1994) could be explained by the fast time constant of Na^+ channel inactivation relative to the membrane time constant and by the asymmetry of membrane charging from dendrite versus soma.

The contradictory conclusions of Regehr et al. (1993), that spikes may be dendritically initiated, could be reconciled with the model by invoking a maturational increase in dendritic Na^+ channel density (Huguenard et al., 1988; Cummins et al., 1994) that might accompany the difference in the ages of rats used in the two studies. With regard to the resolution of this issue, the model makes a number of specific predictions: first, with dendritic spike initiation, the form of dendritic spikes should be biphasic (Figures 9 and 10); second, conditions that favor dendritic spike initiation should lead to nondecremental amplitude spikes in dendrites; third, when it becomes possible to measure accurately the initial segment Na^+ channel density, it should be orders of magnitude larger than the somato-dendritic density; finally, if it were possible to inactivate the axon hillock and initial segment, a profound change in spike initiation should be seen. The last experiment may be extremely difficult due to the close apposition of the hillock to the soma.

Most recent models of cortical and hippocampal pyramidal cells and Purkinje cells have neglected the axon initial segment, typically assigning high density of Na^+ channels to the soma (Bernander et al., 1991; Lytton and Sejnowski, 1991; Traub et al., 1991; De Schutter and Bower, 1994; Rhodes and Gray, 1994). In this study, we have found that the axon hillock and initial segment are of critical importance for spike initiation.

A primary distinguishing feature of the initial segment of the neocortical pyramidal cell, shared with the nodes of Ranvier, is the presence of an electron-dense undercoating (Peters et al., 1968). It has long been speculated that this undercoating is related to electrical conduction (Peters et al., 1968; Palay et al., 1968), possibly relating to an elevated density of Na^+ channels. The existence of a diffusional barrier in the membrane between axon hillock and soma (Srinivasan et al., 1988; Kobayashi et al., 1992) could provide the molecular basis for the trapping of channels in the initial segment.

The initial segment was proposed some time ago as the site for action potential initiation in spinal motoneurons (Coombs et al., 1957; Frank and Fuortes, 1957). Yet the demonstration of active currents in the dendrites of cortical pyramidal neurons left the applicability of the classical model to these cells uncertain. Our model expands upon the pioneering models of Cooley and Dodge (1966; Dodge and Cooley, 1973) and Moore et al. (1983) concerning the locus of spike initiation in the spinal motoneuron. Dodge and Cooley (1973) used a high Na^+ channel density in the initial segment and changed the Na^+ (and K^+) kinetics to reduce threshold there. A shift in the voltage dependence of channel kinetics could theoretically be caused by polarization differences between somatic and neuritic membrane (Bedlack et al., 1994) or by differences in Na^+ channel subtype expression (Westenbroek et al., 1989) or phosphorylation state (Li et al., 1992; Murphy et al., 1993). Experiments by Moore and Westerfield (1983) argued
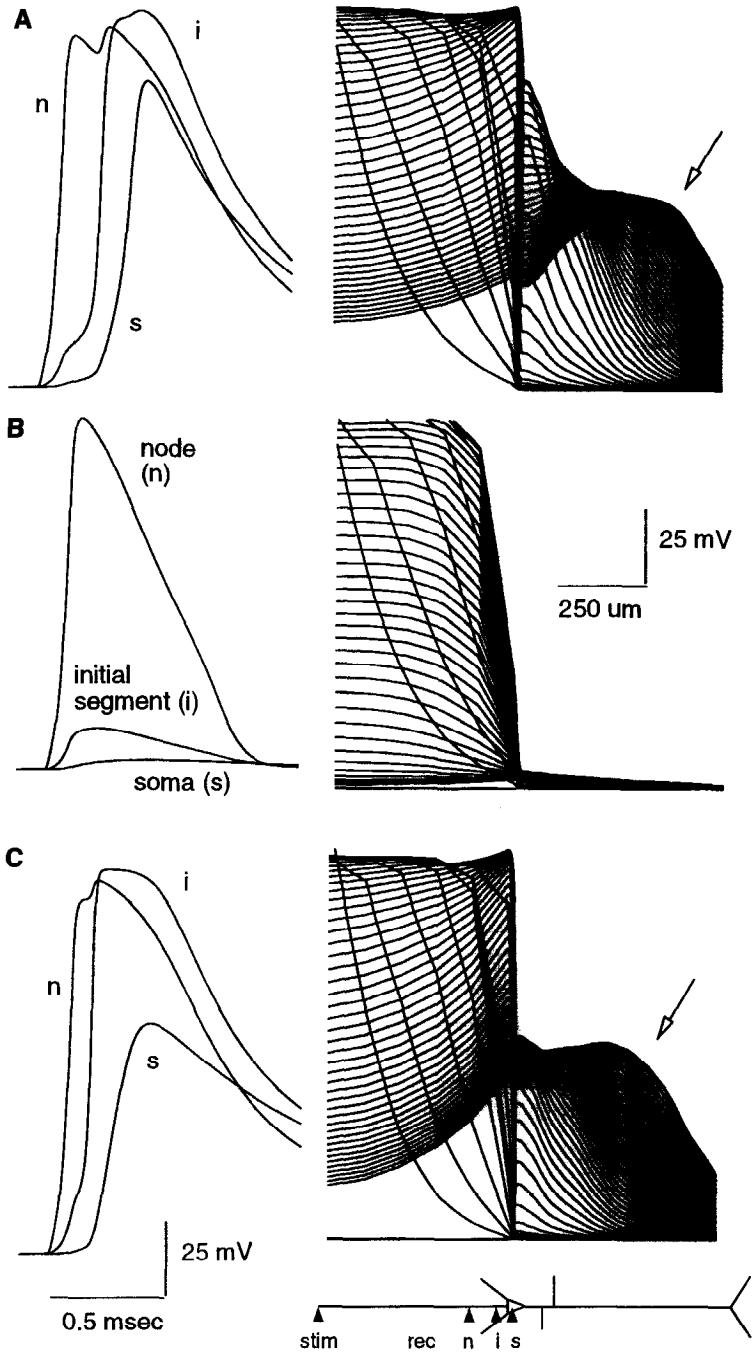
Figure 8. Antidromic Invasion

A current step (0.5 nA, 0.5 ms) was applied to the tip of the axon (>500 μm from soma) to evoke an antidromic action potential. Traces on the left show voltage time courses at the first node of Ranvier (n), the distal end of the initial segment (i), or the soma (s). Curves on the right show voltage as a function of distance from the soma at time steps of 0.1 ms. (A) In the standard model, full invasion of the soma occurs. (B) Na⁺ channels are redistributed evenly through the soma and initial segment rather than being concentrated in the initial segment. Somatic invasion fails. (C) The taper of the hillock is eliminated and its Na⁺ density increased to compensate. Note that somatic spike amplitude is decreased, but dendritic invasion is not compromised (compare [A] and [C] at arrows).

against such axonal specialization. Accordingly, Moore et al. (1983) used identical kinetics and channel densities to the soma and initial segment and found that the initial segment could be the site of initiation, owing solely to the large ratio of the Na⁺ conductance to the passive electrical load there.

A recent model of the hippocampal CA3 pyramidal cell by Traub et al. (1994) incorporated an initial segment with high Na⁺ channel density and Na⁺ channel kinetics distinct from those in the soma and dendrites. In the CA3 model, as in the present study, dendritic stimuli produced spikes that originated at the initial segment and antidromically

invaded the dendritic tree. However, in contrast to our results, axonal initiation in the CA3 model was demonstrated only with channel distributions that restricted Na⁺ conductances to the promixal dendrites and only when the size of stimuli was limited (Traub et al., 1994).

In the present model, the initial segment was critical in spike initiation. Because of the very high Na⁺ channel density (compared with the soma or dendrites), the initial segment actually supplied a significant fraction of the depolarizing current observed at the soma during an action potential. Without the contribution of current from the initial segment, the amplitude of action potentials generated in
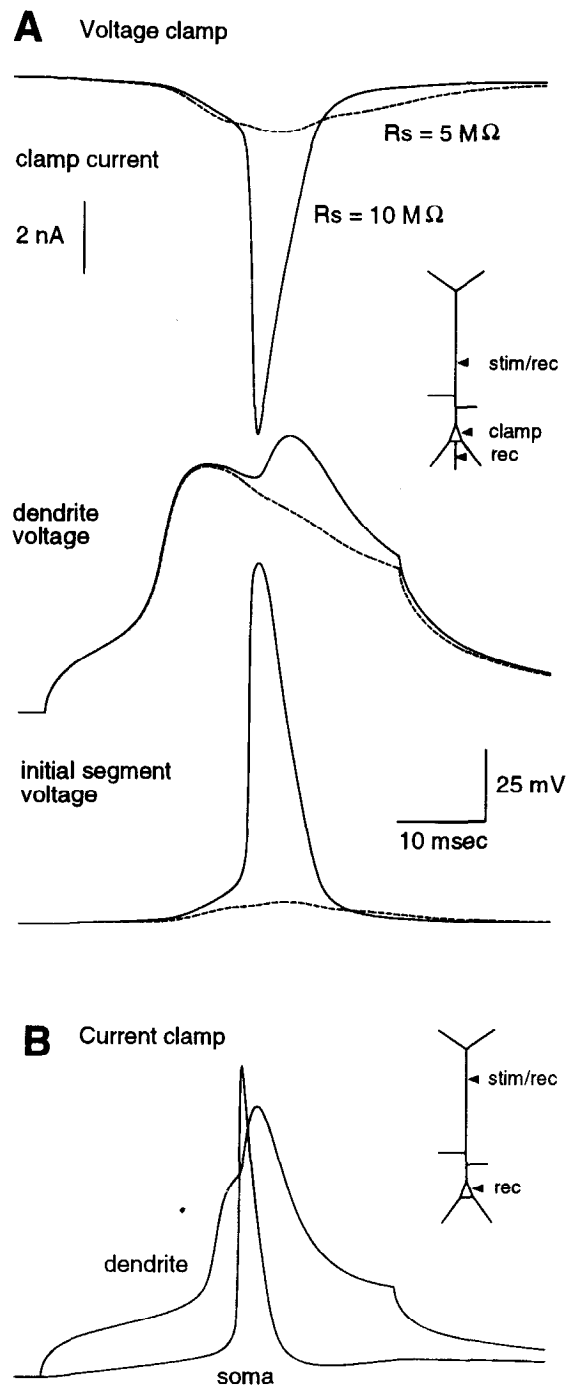
A   Voltage clamp

clamp current

2 nA

Rs = 5 MΩ

Rs = 10 MΩ

stim/rec

clamp rec

dendrite
voltage

initial segment
voltage

25 mV

10 msec

B   Current clamp

stim/rec

rec

dendrite

soma

Figure 9. Voltage Clamp during Dendritic Current Injection

With higher dendritic Na⁺ channel density (90 pS/μm²), an action potential was initiated in the apical dendrite by current injection (300 pA). (A) A somatic voltage clamp showed a small regenerative current caused by the dendritic spike or a much larger regenerative current caused by a subsequent initial segment spike depending on the series resistance of the clamp (top: voltage-clamp current; middle: dendritic voltage at injection site; bottom: voltage at initial segment; solid lines, 5 MΩ; dashed lines, 10 MΩ). Note strong voltage escape at both dendritic and initial segment sites.

(B) The same dendritic Na⁺ channel density and stimulus under current-clamp recording elicited an action potential in the apical dendrite that preceded that in the axon.
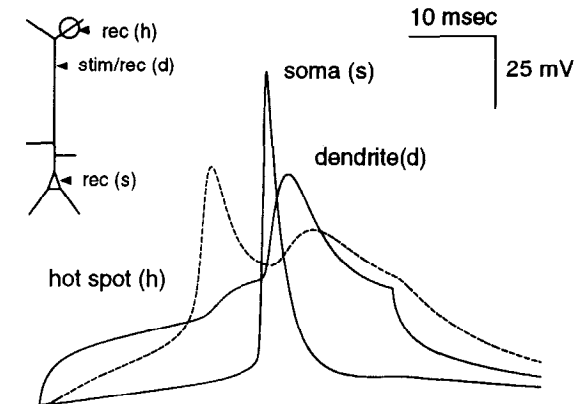

rec (h)

stim/rec (d)

rec (s)

hot spot (h)

10 msec

soma (s)

25 mV

dendrite(d)

Figure 10. Dendritic Spike Initiation by Na⁺ Channel "Hot Spots"

A hot spot of high Na⁺ channel density (300 pS/μm²) was placed on a fine branch in the distal apical tuft (0.8 μm diameter, 34 μm length; 719 μm from the soma). Current injection into the main apical trunk (210 pA) initiated an action potential at the hot spot. Note that the spike failed to propagate into the apical trunk and several milliseconds later a spike was initiated in the initial segment.

the soma was quite small. This result may be comparable to recordings of dissociated pyramidal cells in acute cultures (Hamill et al., 1991), which often showed small action potentials and lack of sustained firing. In these studies, a correlation between spike amplitude and the presence of an apparent axon was noted (J. R. H., unpublished data).

The electrical isolation and high Na⁺ current density of the initial segment from the soma made voltage control of spike initiation very difficult. Once the initial segment became depolarized sufficiently to activate its Na⁺ channels, somatic voltage clamp was completely ineffective in preventing spike initiation. Because spike initiation does not occur in the soma (as tends to be casually assumed) a somatic voltage clamp suffers a severe space-clamp problem in controlling large regenerative Na⁺ currents even under optimal voltage-clamp conditions (Regehr et al., 1993). Thus, the properties of the spike generation zone make interpretation of the locus of origin of unclamped regenerative events difficult (e.g., see Regehr et al., 1992). It is also important to point out that when the soma has been voltage clamped at potentials sufficiently depolarized to inactivate Na⁺ channels in the initial segment, unclamped action potentials continue to be generated from more distal nodes in the axon where passive electrical attenuation brings the membrane potential just to a threshold level. The apparent cessation of somatic action potentials when a neuron is clamped to positive potentials—as for example during a pairing procedure used to induce long-term potentiation (e.g. Malinow and Tsien, 1990; Schuman and Madison, 1994)—does not indicate that the cell has stopped firing.

The geometry of the axon hillock and initial segment and the high axonal Na⁺ channel density enhanced the security with which action potentials from the axon successfully invaded the soma and dendritic compartments. The properties of the myelinated axon beyond the initial segment may also be important to antidromic invasion,

as suggested by Moore et al. (1983). The security of anti-dromic invasion may be functionally significant if action potentials are naturally generated axonally. Although we do not know of any direct evidence for this phenomenon, distal spike initiation followed by retrograde invasion is one possible interpretation of several studies reporting unexplained retrograde synaptic effects (Vincent and Marty, 1993; Pitler and Alger, 1994; Schuman and Madison, 1994).

Finally, the nature of the spike initiation zone may influence the reliability of spike initiation. Because of the stochastic nature of single channel behavior and finite channel numbers, action potential currents might theoretically be affected by single channel conductance fluctuations (Skaugen, 1980). Modeling studies predict that these effects would be greatest in situations involving few channels and small electrical compartments (Skaugen, 1980). Although the initial segment is small and isolated electrically from the soma, the very high total number of Na^+ channels would be expected to effectively wash out single channel stochasticity. This prediction is in accord with the observed reliability of action potential generation in neocortical neurons (Mainen and Sejnowski, 1995). It remains possible that dendritic spike initiation, in regions with a much lower channel density, would be subject to greater stochastic effects.

Experimental Procedures

A multicompartmental single-neuron model was implemented using the simulation program Neuron (Hines, 1993). The fully implicit backward Euler integration method was used with a time step of 25 μs (unless otherwise noted).

Dendritic Anatomy

The dendritic morphology was based on a layer 5 pyramidal neuron from a postnatal day 19 rat (D. Smetters and S. Nelson, unpublished data) filled with biocytin and digitally reconstructed using the Eutectics tracing system (Figure 1A). A spatial discretization of ≤50 μm per compartment was observed for all dendritic segments except the main apical trunk, which was discretized at ≤10 μm per compartment.

The geometry of this cell was similar to measurements from other rat layer 5 pyramidal cells. The soma area was 1,578 μm², comparable to a reported average area of 1,393 μm² (Mason and Larkman, 1990). The apical trunk tapered from 4.5 to 1.4 μm between 100 and 600 μm from the soma, again similar to reported measurements (Larkman and Mason, 1990). This required a slight correction of the trunk diameter of the original reconstruction to obtain a more uniform taper. The total dendritic length was 13,654 μm (6,704 μm basal, 4,167 μm apical oblique, 2,226 μm apical tuft, 557 μm apical trunk). The median overall dendritic diameter was ~0.75 μm.

Dendritic spines were taken into account by increasing the effective membrane area (Stratford et al., 1989); see Electrical Properties below Single spine area was 0.83 μm (Harris and Stevens, 1989). Densities were assigned to different areas based on spine counts per linear micrometer from rat layer 5 pyramids (Larkman, 1991). The total dendritic membrane area was 36,344 μm² before and 54,080 μm² after incorporation of spines.

Axonal Anatomy

A myelinated axon was attached to the soma of the neuron. The geometry of the initial segment (the unmyelinated segment of the axon closest to the soma) and axon hillock—the transitional zone between the soma and initial segment proper (Palay et al., 1968), here used to refer to the proximal, tapering portion of the initial segment—have been documented in serial electron microscopic reconstructions for cat corti-

cal pyramidal cells (Fariñas and DeFelipe, 1991). The average length of the initial segment from this study is ~20 μm and the average diameter ~1 μm, tapering from the proximal to the distal end. Similar diameters have been reported in rat neocortex (Westrum, 1970). Based on these data, our standard model consisted of a 10 μm hillock tapering from 4 to 1 μm followed by a 15 μm initial segment of 1 μm diameter (see Figure 1B). Both hillock and initial segment were divided lengthwise into 10 segments for simulation.

Myelination begins immediately at the end of the initial segment (Fariñas and DeFelipe, 1991). Measurements of cerebral axon diameters are in the range of 0.5–2 μm (Haug, 1968). The initial segment (and nodes of Ranvier) are generally narrower than myelinated internodal segments of the axon (Palay et al., 1968). We assumed an internode diameter of 1.5 μm and node diameter of 1 μm. Internode lengths were 100 μm, comparable to measurements of the terminal arbors of cat cortical axons (Deschênes and Landry, 1980). Nodes themselves were 1 μm in length. Internodes were divided into 25 segments, and nodes were a single segment.

Electrical Properties

Membrane capacitance (C_m) is often assumed to be 1 μF/cm² but is probably lower, in the range 0.6–0.8 μF/cm² (Major et al., 1994). We used a value of 0.75 μF/cm². A membrane resistance of 40 kΩ-cm² and axial resistance of 200 Ω-cm are in line with recent modeling studies based on patch recordings (Major et al., 1994; Spruston et al., 1994). These values gave a membrane time constant of 30 ms and an input resistance of 74.2 MΩ. Simulations were run to examine the sensitivity of the results to the specific electrical constants and were found to be insignificant to the results described.

The electrical properties of the axon are more difficult to estimate. In the absence of better evidence, we assumed identical parameters to the dendritic membrane, with two exceptions. First, capacitance of the myelinated segments is much lower than unmyelinated membrane (Black et al., 1990). Second, the membrane resistance of the nodes is believed to be substantially lower than other membrane (Black et al., 1990), helping to repolarize the membrane following an action potential in the absence of a delayed rectifier current. In line with other axon models (Graham and Redman, 1994), we chose $R_{m-node} = 50$ Ω-cm² and $C_{m-myelin} = 0.04$ μF/cm². The electrical properties are summarized in Table 1.

Channel Kinetics

We assumed that the primary contribution to the initiation and propagation of single action potentials is made by the fast Na^+ channel. Although there are also dendritic voltage-dependent Ca^{2+} channels (Amitai et al., 1993; Yuste et al., 1994), these were not included in the model. As the model was not required to produce repetitive firing, other K^+ channels that sculpt such behavior were omitted. We used a single noninactivating, voltage-dependent K^+ current to provide spike repolarization. No other channels were included.

The kinetics of the Na^+ currents were based on data obtained from acutely isolated rat neocortical neurons (Huguenard et al., 1988; Hamill et al., 1991) and were very similar to those reported in rat brain Na^+ channel expressed in oocytes (Stühmer et al., 1987) and rat and human neocortex (Cummins et al., 1994). We reanalyzed the original data of Hamill et al. (1991) to obtain the kinetics used. As these measurements

Table 1. Parameters for the Equations describing the Na^+ and K^+ Currents

Current	Variable	Function	A	$V_{1/2}$	k
I_{Na}	m	α	0.182	−35	9
		β	0.124	−35	9
	h	α	0.024	−50	5
		β	0.0091	−75	5
		∞	–	−65	6.2
I_K	m	α	0.02	20	9
		β	0.002	20	9

Refer to equations 3 and 4 in the text.

and the experiments of Stuart and Sakmann (1994) and Regehr et al. (1993) were performed at room temperature, no adjustment of kinetics for temperature was necessary. The voltage dependence of the kinetics was uniformly shifted ~5 mV depolarized in order to obtain a higher threshold.

The equations for the Na$^+$ current were based on those of Hodgkin and Huxley (1952) and were similar but not identical to those used by McCormick and Huguenard (1992). The Na$^+$ current was calculated using the standard ohmic relation

$$I_{Na} = \bar{g}_{Na}\, m^3\, h\, (V_m - E_{Na}), \tag{1}$$

where I_{Na} is the Na$^+$ current, V_m is the membrane potential, E_{Na} is the equilibrium potential for Na$^+$ (assumed to be +60 mV), and m and h are the activation and inactivation state variables, respectively. The variable m ranges from 0 (not activated) to 1 (fully activated), and h ranges from 0 (fully inactivated) to 1 (no inactivation). The maximal conductance is the product $\bar{g}_{Na} = \gamma_{Na}\rho_{Na}$, where γ_{Na} is the single channel conductance and ρ_{Na} is the channel density. I_{Na} activation was described by the usual first order kinetic reaction, open $\rightleftharpoons$ closed, which yields steady-state value m_∞ time constant τ_m given by

$$m_\infty = \frac{\alpha}{\alpha + \beta}$$

$$\tau_m = \frac{1}{\alpha + \beta}, \tag{2}$$

where α and β, the forward (opening) and backward (closing) reaction rates, respectively, are functions of the local membrane potential. Specifically,

$$\alpha(V_m) = \frac{A\,(V_m - V_{1/2})}{1 - e^{-(V_m - V_{1/2})/k}}$$

$$\beta(V_m) = \frac{-A(V_m - V_{1/2})}{1 - e^{(V_m - V_{1/2})/k}}, \tag{3}$$

where the A is a rate constant, $V_{1/2}$ is the half-activation voltage, and k determines the slope of the activation curve. In contrast, I_{Na} inactivation was best described with independent functions for time constant and steady-state values. Thus, τ_h was described analogously to τ_m, but m_∞ was given directly by

$$h_\infty = \frac{1}{1 + e^{(V_m - V_{1/2})k}}. \tag{4}$$

The parameters for equations 3 and 4 were derived from the data of Hamill et al., 1991, and are given in Table 2 of this study. The steady-state and time-constant voltage dependencies are shown in Figure 2. The peak open probability (P_{open}) was 0.53 (during a step from −90 to +50 mV). A peak current of ~1 pA/μm^2 occurred during voltage clamp

Table 2. Membrane Parameters Used in the Standard Model

Parameter	Symbol	Region	Value	Units
Resting potential	V_{rest}		−70	mV
Axial resistivity	R_{ax}		200	Ω-cm
Membrane capacitance	C_m	soma/dend	0.75	μF/cm^2
		node	0.75	μF/cm^2
		myelin	0.04	μF/cm^2
Membrane resistivity	R_m	soma/dend	40,000	Ω-cm^2
		node	50	Ω-cm^2
		myelin	40,000	Ω-cm^2
Na$^+$ conductance density	$\bar{g}_{Na}$	soma/dend	30	pS/μm^2
		node	30,000	pS/μm^2
		myelin	30	pS/μm^2
K$^+$ conductance density	$\bar{g}_K$	soma/basal	100	pS/μm^2
		elsewhere	0	pS/μm^2

"Node" indicates the axon hillock, initial segment, and nodal membranes.

steps from −90 to −10 mV. At rest (−70 mV), 31% of channels were inactivated.

The equations we used to describe the Na$^+$ activation function were similar in form to those used in most modeling studies. However, the steepness of the activation curve was notably shallower in ours than in many others (Bernander et al., 1991; Lytton and Sejnowski, 1991; De Schutter and Bower, 1994; Rhodes and Gray, 1994; Traub et al., 1994). The decreased slope in the present study is in accord with the data we analyzed (Hamill et al., 1991), as well as other experimental reports (Belluzzi and Sacchi, 1986; Stühmer et al., 1987; Huguenard et al., 1988; Sah et al., 1988; Cummins et al., 1994). Although the steeper slope apparently is adequate for most purposes, a shallower slope had significant effects in the more detailed model examined here, increasing the disparity between axonal and dendritic threshold levels.

A noninactivating K$^+$ current was described by

$$I_K = \bar{g}_K\, m\, (V_m - E_K), \tag{6}$$

where E_K was −90 mV. Activation kinetics were analogous to the Na$^+$ activation variable (equations 2 and 3), with parameters given in Table 1.

Channel Distributions

Comparisons between dendritic and somatic Na$^+$ channel densities in neocortical pyramids have been made by whole-cell (Huguenard et al., 1989) and patch recordings (Huguenard et al., 1989; Stuart and Sakmann, 1994). Neither study found a difference between somatic and dendritic densities. We therefore assumed a uniform density of Na$^+$ channels throughout the soma and dendritic membrane. Somatic and dendritic channel density in the model were adjusted in order to match the amplitude and latency distributions reported by Stuart and Sakmann (1994). We arrived at a maximal Na$^+$ conductance of 30 pS/μm^2. A 3-fold higher density (90 pS/μm^2) was used to reproduce results of Regehr et al., 1993. These values are comparable to estimated somatic/dendritic Na$^+$ conductance densities of 40–120 pS/μm^2 (Huguenard et al., 1989; Stuart and Sakmann, 1994).

Given the relatively low channel open probability during simulated voltage-clamp steps, the effective Na$^+$ current density in the model appears to be lower than experimental reports: model current density of 1–3 pA/μm^2 compared with 4.6 pA/μm^2 in cell-attached patches (Stuart and Sakmann, 1994). At least three factors may contribute to this quantitative discrepancy. First, Na$^+$ current densities in outside-out patches may be larger than in intact cells because Na$^+$ concentrations in the patch pipette (2 mM; Stuart and Sakmann, 1994) are significantly lower than normal intracellular concentrations (10–30 mM; Erecinska and Silver, 1989). Second, measurements of area of patches in which Na$^+$ currents were measured were not available, and an area of 1.5 μm^2 (Stuart and Sakmann, 1994) may underestimate the true patch area. Third, Na$^+$ channels are down-regulated by protein kinase C, cAMP-dependent protein kinase, and phosphoprotein phosphotases (Li et al., 1992; Murphy et al., 1993). The absence of these enzymes in the outside-out patch configuration may therefore lead to an increase in channel activity in patches compared with intact cells.

Na$^+$ channel density in the initial segment and nodes of Ranvier have been shown to be large compared with the internodal, somatic, and dendritic membrane (Wollner and Catterall, 1986; Chiu and Schwarz, 1987; Angelides et al., 1988; Black et al., 1990; Waxman and Ritchie, 1993). We assumed an internodal density identical to the somatic/dendritic density of 30 pS/μm^2. Conventional estimates for nodal Na$^+$ channel density are around 1000–2000 channels/μm^2 (reviewed in Waxman and Ritchie, 1993). Assuming a similarity between initial segment and nodes of Ranvier, which have the same ultrastructural features (Palay et al., 1968; Peters et al., 1968), we used a value of 30,000 pS/μm^2 for the initial segment and nodal membrane, corresponding to 1,500–2,000 channels/μm^2 at 15–20 pS single channel conductance (Stühmer et al., 1987; Alzheimer et al., 1993).

K$^+$ channel densities are less well known. We assumed a uniform low density throughout the soma and basal dendrites: 100 pS/μm^2. This was chosen to give weak but complete spike repolarization with minimal activation below action potential threshold in order not to interfere with initiation. No significant differences in the results were found

when K$^+$ channels were restricted to the soma and/or initial segment (data not shown). It was necessary to exclude fast K$^+$ channels from the apical dendrites in order to reproduce the recordings of Stuart and Sakmann (1994), which show extremely slow repolarization of dendritic action potentials. However, appropriate dendritic repolarization and very similar overall results could also be obtained when low densities of much more slowly activating ($\tau > 25$ ms) noninactivating voltage-dependent K$^+$ channels were present in the apical dendrites (data not shown). Because of the large leak conductance in the nodes of the axon, no voltage-dependent K$^+$ current was necessary for action potential repolarization in the axon (Kaars and Faber, 1981; Graham and Redman, 1994). The channel densities used in the model are summarized along with electrical constants in Table 1.

Acknowledgments

Received May 3, 1995; revised August 16, 1995.

References

Alzheimer, C., Schwindt, P.C., and Crill, W.E. (1993). Modal gating of Na$^+$ channels as a mechanism of persistent Na$^+$ current in pyramidal neurons from rat and cat sensorimotor cortex. J. Neurosci. 13, 660–673.

Amitai, Y., Friedman, A., Connors, B.W., and Gutnick, M.J. (1993). Regenerative electrical activity in apical dendrites of pyramidal cells in neocortex. Cereb. Cortex 3, 26–38.

Angelides, K.J., Elmer, L.W., Loftus, D., and Elson, E. (1988). Distribution and lateral mobility of voltage-dependent sodium channels in neurons. J. Cell Biol. 106, 1911–1924.

Bedlack, R.S., Jr., Wei, M.-d., Fox, S.H., Gross, E., and Loew, L.M. (1994). Distinct electric potentials in soma and neurite membranes. Neuron 13, 1187–1193.

Belluzzi, O., and Sacchi, O. (1986). A quantitative description of the sodium current in the rat sympathetic neurone. J. Physiol. 380, 275–291.

Bernander, Ö., Douglas, R.J., Martin, K.A.C., and Koch, C. (1991). Synaptic background activity influences spatiotemporal integration in single pyramidal cells. Proc. Natl. Acad. Sci. USA 88, 11569–11573.

Black, J.A., Kocsis, J.D., and Waxman, S.G. (1990). Ion channel organization of the myelinated fiber. Trends Neurosci. 13, 48–54.

Chiu, S.Y., and Schwarz, W. (1987). Sodium and potassium currents in acutely demyelinated internodes of rabbit sciatic nerves. J. Physiol. 391, 631–649.

Cooley, J.W., and Dodge, F.A. (1966). Digital computer simulations for excitation and propagation of the nerve impulse. Biophys. J. 6, 583–599.

Coombs, J.S., Curtis, D.R., and Eccles, J.C. (1957). The generation of impulses in motoneurones. J. Physiol. 139, 232–249.

Cowan, R.L., and Wilson, C.J. (1994). Spontaneous firing patterns and axonal projections of single corticostriatal neurons in the rat medial agranular cortex. J. Neurophysiol. 71, 17–32.

Cummins, T.R., Xia, Y., and Haddad, G.G. (1994). Functional properties of rat and human neocortical voltage-sensitive sodium currents. J. Neurophysiol. 71, 1052–1064.

De Schutter, E., and Bower, J.M. (1994). An active membrane model of the cerebellar Purkinje cell. I. Simulation of current clamps in slice. J. Neurophysiol. 71, 375–400.

Deschênes, M., and Landry, P. (1980). Axonal branch diameter and spacing of nodes in the terminal arborization of identified thalamic and cortical neurons. Brain Res. 191, 538–544.

Dodge, F.A., and Cooley, J.W. (1973). Action potential of the motorneuron. IBM J. Res. Dev. 17, 219–229.

Erecinska, M., and Silver, I.A. (1989). ATP and brain function. J. Cereb. Blood Flow Metab. 9, 2–19.

Fariñas, I., and DeFelipe, J. (1991). Patterns of synaptic input on corticocortical and corticothalamic cells in the cat visual cortex. II. The axon initial segment. J. Comp. Neurol. 304, 70–77.

Frank, K., and Fuortes, M.G.F. (1957). Presynaptic and postsynaptic inhibition of monosynaptic reflexes. Fed. Proc. 16, 39–40.

Gogan, P., Gueritaud, J.P., and Tyc-Dumont, S. (1983). Comparison of antidromic and orthodromic action potentials of identified motor axons in the cat's brain stem. J. Physiol. 335, 205–220.

Graham, B., and Redman, S. (1994). A simulation of action potentials in synaptic boutons during presynaptic inhibition. J. Neurophysiol. 71, 538–549.

Hamill, O.P., Huguenard, J.R., and Prince, D.A. (1991). Patch-clamp studies of voltage-gated currents in identified neurons of the rate cerebral cortex. Cereb. Cortex 1, 48–61.

Harris, K.M., and Stevens, J.K. (1989). Dendritic spines of CA1 pyramidal cells in the rat hippocampus: serial electron microscopy with reference to their biophysical characteristics. J. Neurosci. 9, 2982–2997.

Haug, H. (1968). Quantitative Elektronenmikroskopische untersuchungen über den markfaseraufbau in der Sehrinde der Katze. Brain Res. 11, 65–84.

Hines, M. (1993). Neuron—a program for simulation of nerve equations. In Neural Systems: Analysis and Modeling, F.H. Eeckman, ed. (Boston: Kluwer Academic Publishers), pp. 127–136.

Hodgkin, A.L., and Huxley, A.F. (1952). A quantitative description of membrane current and its application to conduction and excitation in nerve. J. Physiol. 117, 500–544.

Huguenard, J.R., Hamill, O.P., and Prince, D.A. (1988). Developmental changes in Na$^+$ conductances in rat neocortical neurons: appearance of a slowly inactivating component. J. Neurophysiol. 59, 778–794.

Huguenard, J.R., Hamill, O.P., and Prince, D.A. (1989). Sodium channels in dendrites of rat cortical pyramidal neurons. Proc. Natl. Acad. Sci. USA 86, 2473–2477.

Jester, J.M., Campbell, L.W., and Sejnowski, T.J. (1995). Associative EPSP-spike potentiation induced by pairing orthodromic and antidromic stimulation in rat hippocampal slices. J. Physiol. 484, 689–705.

Kaars, C., and Faber, D.S. (1981). Myelinated central vertebrate axon lacks voltage-sensitive potassium conductance. Nature 212, 1063–1065.

Kobayashi, T., Storrie, B., Simons, K., and Dotti, C.G. (1992). A functional barrier to movement of lipids in polarized neurons. Nature 359, 647–650.

Larkman, A.U. (1991). Dendritic morphology of pyramidal neurones of the visual cortex of the rat. III. Spine distributions. J. Comp. Neurology 306, 332–343.

Larkman, A.U., and Mason, A. (1990). Correlations between morphology and electrophysiology of pyramidal neurons in slices of rat visual cortex. I. Establishment of cell classes. J. Neurosci. 10, 1407–1414.

Li, M., West, J.W., Lai, Y., Scheuer, T., and Catterall, W.A. (1992). Functional modulation of brain sodium channels by cAMP-dependent phosphorylation. Neuron 8, 1151–1159.

Lytton, W.W., and Sejnowski, T.J. (1991). Simulations of cortical pyramidal neurons synchronized by inhibitory interneurons. J. Neurophysiol. 66, 1059–1079.

Magee, J.C., and Johnston, D. (1995). Synaptic activation of voltage-gated channels in the dendrites of hippocampal pyramidal neurons. Science 268, 301–304.

Mainen, Z.F., and Sejnowski, T.J. (1995). Reliability of spike timing in neocortical neurons. Science 268, 1503–1506.

Major, G., Larkman, A.U., Jonas, P., Sakmann, B., and Jack, J.J. (1994). Detailed passive cable models of whole-cell recorded CA3 pyramidal neurons in rat hippocampal slices. J. Neurosci. 14, 4613–4638.

Malinow, R., and Tsien, R.W. (1990). Presynaptic enhancement shown by whole-cell recordings of long-term potentiation in hippocampal slices. Nature 346, 177–180.

Mason, A., and Larkman, A.U. (1990). Correlations between morphology and electrophysiology of pyramidal neurons in slices of rat visual cortex. II. Electrophysiology. J. Neurosci. 10, 1415–1428.

Moore, J.W., and Westerfield, M. (1983). Action potential propagation and threshold parameters in inhomogeneous regions of squid axons. J. Physiol. 336, 285–300.

Moore, J.W., Stockbridge, N., and Westerfield, M. (1983). On the site of impulse generation in a neurone. J. Physiol. 336, 301–311.

Murphy, B.J., Rossie, S., DeJongh, K.S., and Catterall, W.A. (1993). Identification of the sites of selective phosphorylation and dephosphorylation of the rat brain Na$^+$ channel alpha subunit by cAMP-dependent protein kinase and phosphoprotein phosphatases. J. Biol. Chem. 268, 27355–27362.

Palay, S.L., Sotelo, C., Peters, A., and Orkland, P.M. (1968). The axon hillock and the initial segment. J. Cell Biol. 37, 193–201.

Peters, A., Proskauer, C.C., and Kaiserman-Abramof, I.R. (1968). The small pyramidal neuron of the rat cerebral cortex: the axon hillock and the initial segment. J. Cell Biol. 39, 604–619.

Pitler, T.A., and Alger, B.E. (1994). Depolarization-induced suppression of GABAergic inhibition in rat hippocampal pyramidal cells: G protein involvement in a presynaptic mechanism. Neuron 13, 1447–1455.

Regehr, W.G., Konnerth, A., and Armstrong, C.M. (1992). Sodium action potentials in the dendrites of cerebellar Purkinje cells. Proc. Natl. Acad. Sci. USA 89, 5492–5496.

Regehr, W., Kehoe, J., Ascher, P., and Armstrong, C. (1993). Synaptically triggered action potentials in dendrites. Neuron 11, 145–151.

Rhodes, P.A., and Gray, C.M. (1994). Simulations of intrinsically bursting neocortical pyramidal neurons. Neural Comp. 6, 11086–11100.

Sah, P., Gibb, A.J., and Gage, P.W. (1988). The sodium current underlying action potentials in guinea pig hippocampal CA1 neurons. J. Gen. Physiol. 91, 373–398.

Schuman, E.M., and Madison, D.V. (1994). Locally distributed synaptic potentiation in the hippocampus. Science 263, 532–536.

Skaugen, E. (1980). Firing behavior in nerve cell models with a two-state pore system. Acta. Physiol. Scand. 109, 377–392.

Softky, W. (1995). Simple codes versus efficient codes. Curr. Opin. Neurobiol. 5, 239–247.

Spruston, N., Jaffe, D.B., and Johnston, D. (1994). Dendritic attenuation of synaptic potentials and currents: the role of passive membrane properties. Trends Neurosci. 17, 161–164.

Srinivasan, Y., Elmer, L., Davis, J., Bennett, V., and Angelides, K. (1988). Ankyrin and spectrin associate with voltage-dependent sodium channels in brain. Nature 333, 177–180.

Stratford, K., Mason, A., Larkman, A., Major, G., and Jack, J.J.B. (1989). The modeling of pyramidal neurones in the visual cortex. In The Computing Neuron, R. Durbin, C. Miall, and G. Mitchison, eds. (London: Addison-Wessley).

Stuart, G.J., and Sakmann, B. (1994). Active propagation of somatic action potentials into neocortical pyramidal cell dendrites. Nature 367, 69–72.

Stühmer, W., Methfessel, C., Sakmann, B., Noda, M., and Numa, S. (1987). Patch clamp characterization of sodium channels expressed from rat brain cDNA. Eur. Biophys. J. 14, 131–138.

Traub, R.D., Wong, R.K.S., Miles, R., and Michelson, H. (1991). A model of a CA3 hippocampal pyramidal neuron incorporating voltage-clamp data on intrinsic conductances. J. Neurophysiol. 66, 635–650.

Traub, R.D., Jefferys, J.G.R., Miles, R., Whittington, M.A., and Toth,

K. (1994). A branching dendrite model of a rodent CA3 pyramidal neurone. J. Physiol. 481, 79–95.

Vincent, P., and Marty, A. (1993). Neighboring cerebellar Purkinje cells communicate via retrograde inhibition of common presynaptic interneurons. Neuron 11, 885–893.

Waxman, S.G., and Ritchie, J.M. (1993). Molecular dissection of the myelinated axon. Ann. Neurol. 33, 121–136.

Westenbroek, R.E., Merrick, D.K., and Catterall, W.A. (1989). Differential subcellular localization of the R$_I$ and R$_{II}$ Na$^+$ channel subtypes in central neurons. Neuron 3, 695–704.

Westrum, L.E. (1970). Observations on the initial segments of axons in the prepyriform cortex of the rat. J. Comp. Neurol. 139, 337–356.

Wollner, D.A., and Catterall, W.A. (1986). Localization of sodium channels in axon hillocks and initial segments of retinal ganglion cells. Proc. Natl. Acad. Sci. USA 83, 8424–8428.

Yuste, R., Gutnick, M.J., Saar, D., Delaney, K.R., and Tank, D.W. (1994). Ca^{2+} accumulations in dendrites of neocortical pyramidal neurons: an apical band and evidence for two functional compartments. Neuron 13, 23–43.